Supporting information
Fully alloyed metal nanorods with highly tunable properties

Wiebke Albrecht[1*†], Jessi E.S. van der Hoeven[1,2†], Tian-Song Deng[1], Petra E. de Jongh[2], and Alfons van Blaaderen [1*]

[1]*Soft Condensed Matter, Debye Institute for Nanomaterials Science, Utrecht University, Princetonplein 5, 3584 CC Utrecht, The Netherlands*
[2]*Inorganic Chemistry and Catalysis, Debye Institute for Nanomaterials Science, Utrecht University, Universiteitsweg 99, 3584 CG Utrecht, The Netherlands*
[†]These authors contributed equally to this work.
[*]To whom correspondence should be addressed.
E-mail: W.Albrecht@uu.nl; A.vanBlaaderen@uu.nl

Methods

Materials

All chemicals were used as received without further purification. Hexadecyltrimethylammonium bromide (CTAB, >98.0%) and sodium oleate (NaOL, >97.0%) were purchased from TCI America. Hydrogen tetrachloroaurate trihydrate ($HAuCl_4$ H_2O), sodium hydroxide (98%), and polyvinylpyrrolidone (PVP, average molecular weight 58000 g/mol, K29-32) were purchased from Acros Organics. L-Ascorbic Acid (BioXtra, ≥99%), silver nitrate ($AgNO_3$,≥99%), sodium borohydride ($NaBH_4$, 99%), hydrochloric acid (HCl, 37 wt% in water), tetraethyl orthosilicate (TEOS, 98%), ammonium hydroxide solution (≥25 wt% in water), sodium tetrachloropalladate-(II) (Na_2PdCl_4, 98%) and potassium tetrachloroplatinate-(II) (K_2PtCl_4, 98%) were purchased from Sigma-Aldrich. Ultrapure water (Millipore Milli-Q grade) with a resistivity of 18.2 MΩ was used in all of the experiments. All glassware for the AuNR synthesis was cleaned with fresh aqua regia (HCl/HNO_3 in a 3:1 volume ratio), rinsed with large amounts of water and dried at 100 °C before usage.

Synthesis of bimetallic core-shell NRs in a mesoporous silica shell

The synthesis of the uncoated AuNRs was done according to the procedure described by X. Ye et al. [1], making use of a binary surfactant mixuture of hexadecyltrimethylammonium bromide (CTAB) and sodium oleate (NaOL). For the silica coating the procedure described by I. Gorelikov and N. Matsuura [2] was followed, whereby the rods were dispersed in an aqueous solution of 1.5 mM CTAB and 0.001 mM NaOH, to which 3 times 0.33 vol% of a 20 vol% TEOS in ethanol solution was added with a 45 minutes time interval between the additons. After 2 days of ageing at 30 °C, while magnetically stirring at 400 rpm, the rods were washed with water and ethanol, and redispersed in methanol (λ_{LSPR}=778 nm, extinction=3.5). In all washing steps we typically used a centrifugation speed of 7000-9000 rcf for 30-10 min, respectively. The average silica shell thickness was 18 nm.

Oxidative etching

The oxidative etching of $Au@SiO_2$ NRs was done similarly to the procedure described by T. Deng et al. [3], but with H_2O_2 instead of air as oxidizing agent for a more controllable and efficient etching of the AuNRs. The H_2O_2 concentration and reaction temperature can be varried to tune the reaction rate of the oxidative etching [4]. Here, 12 mL of $Au@SiO_2$ NRs (λ_{LSPR}=778 nm, extinction=3.5) and 240 μL concentrated HCl (37 vol%) were mixed in a 40 mL glass vial while magnetically stirring at room temperature. 240 μL H_2O_2 in MeOH (0.033 vol%) were added and the reaction mixture was placed in a 70 °C oil bath. After 15 min the reaction mixture was removed from the oil bath and cooled down to room temperature by adding 18 mL fresh MeOH. The

etched particles were washed with 20 mL and redispersed in 12 mL of a 1.1 wt% PVP (K29-32) in H_2O solution, respectively. The resulting LSPR peak position of the etched Au@SiO_2 NRs in PVP/H_2O was 745 nm with an extinction of 2.2.

Metal overgrowth

The etched Au@SiO_2 NRs were overgrown with Ag, Pd or Pt according to the procedure described by T. Deng et al.[3]. 0.3 mL of etched Au@SiO_2 NRs in PVP/H_2O (λ_{LSPR}=745 nm, extinction=2.2) and 30 μL 2 mM $AgNO_3$, 5 mM Na_2PdCl_4 or 10 mM K_2PtCl_4 in water were added to a 4 mL glass vial. Next, 30 μL of 8 and 20 mM ascorbic acid (AA) were added for the Ag- and Pd-shell growth, respectively, and the vial was directly placed into a Vortex Shaker and shaken for 20 min. The extinction spectra before and after metal overgrowth are shown in Figure S1. After recording the spectra the samples were washed with H_2O and redispersed in 1 mL EtOH (100%). Because of partial oxidation and dissolution of the Ag-shell during storage, the Au@Ag@SiO_2 NRs were not used more than two weeks after synthesis. We therefore used different batches of particles for the experiments, which were produced under the same conditions (see Table S1). However, we observed that the stability of the Ag-shell can be significantly improved when storing the core-shell rods in the fridge at 5 °C. It should be mentioned that the described metal overgrowth procedure was done equally successfully in H_2O instead of PVP/H_2O, yielding ligand-free NRs. Besides, we do not expect the PVP molecules to fit inside the silica pores and adsorb onto the metal surface because of their large molecular size, making it relatively easy to wash them away with water and obtain ligand-free nanorods. Furthermore, we checked that alloying also works for the NRs prepared without PVP.

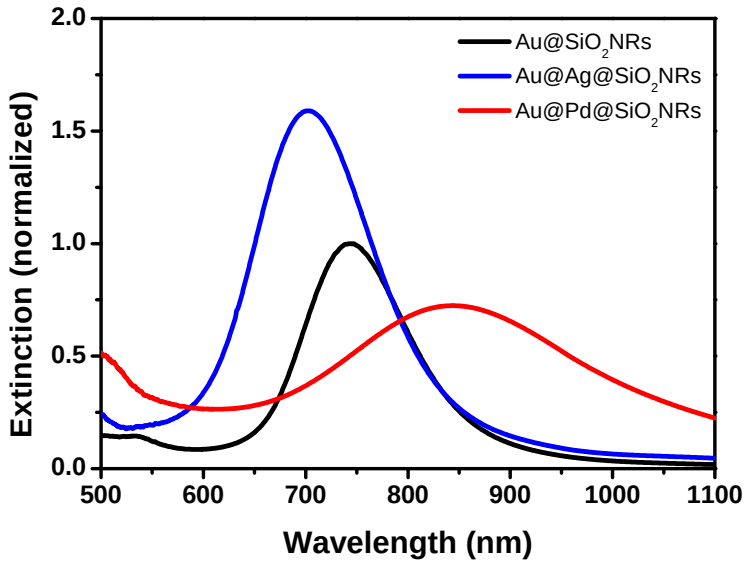

Figure S1: Extinction spectra of the etched Au@SiO_2 NRs (black curve) and after growing a Ag (blue curve) and Pd (red curve) shell. The spectra were recorded in 1.1 wt% PVP in H_2O.

The dimensions and aspect ratios of the NRs before and after oxidative etching and metal overgrowth are summarized in Table S1. We used the same batch of silica coated AuNRs for Ag and Pd overgrowth and a comparable batch of AuNRs for Pt overgrowth. The silica shell thickness is the same for the batches in Table S1 (∼18 nm). It should be noted that an accurate size determination of the Pd shell is difficult since it exhibits a dendritic structure.

Table S1: Dimensions and aspect ratios (AR) of $Au@SiO_2$ NRs before and after etching, $Au@Ag@SiO_2$, $Au@Pd@SiO_2$ and $Au@Pt@SiO_2$ NRs after metal overgrowth, as determined from TEM analysis.

Sample ID	Length (nm)	Diameter (nm)	AR
$Au@SiO_2$ NRs before etching	71	20	3.6
$Au@SiO_2$ NRs after etching	61	20	3.1
$Au@Ag@SiO_2$ NRs used for in-situ heating	74	27	2.7
$Au@Ag@SiO_2$ NRs used for N_2 heating	73	27	2.7
$Au@Ag@SiO_2$ NRs used for air heating	73	27	2.7
$Au@Pd@SiO_2$ NRs used for in-situ heating	73	22	3.3
$Au@Pt@SiO_2$ NRs used for in-situ heating	57	18	3.2

Scaling up

For potential applications it is important to point out that the alloying procedure described in this paper can be scaled up. The main difficulty in scaling up is the colloidal synthesis of a larger amount of core-shell rods and in particular the metal overgrowth of the silica coated AuNRs. The reduction of the metal-precursor (especially $AgNO_3$) by ascorbic acid is usually so fast ($\leq$5 s) that in reaction volumes larger than 1 mL inhomogeneous overgrowth and nucleation of new nanoparticles occurs due to insufficient mixing. Therefore, the reaction rate was slowed down by performing the metal overgrowth at a low pH, allowing to scale the synthesis up by a factor 1000. At a low pH the reduction of the metal precursors by ascorbic is slowed down significantly, because part of the ascorbic acid molecules are in their fully protonated, non reducing form, and slowly converted into its partically deprotonaed, reducing form. Due to the lower reaction rate, ascorbic acid can be homogenously mixed into the dispersion before it reacts with the metal-precursor. Instead of a 300 μL reaction volume the Ag-metal overgrowth was carried out in a 200 mL reaction mixture and a 1.5$\times$ higher AuNR concentration (λ_{LSPR}=748 nm, extinction=3.0), but in principle one could even go to larger reaction volumes or more concentrated AuNR dispersions. In the 200 mL overgrowth procedure 200 mL aqueous etched-$AuNR@SiO_2$ dispersicon was acidified with 1 mL HCl (37%), resulting in a pH of $\sim$1.2. 3 mL 5 mM $AgNO_3$ were added to the mixture, while stirring magnetically with 400 rpm at room temperature. Next, 3 mL 20 mM ascorbic acid was added to the solution. The core-shell nanorods were washed as described above, dispersed in EtOH and dried in a 4 mL glass vial by heating them at 60 °C overnight. Subsequently, the dried $Au@Ag@SiO_2$ NRs were heated to 450 °C in the glass vial under a N_2 flow. After alloying the particles were redispersed in ethanol or ethanol/water by using a sonication bath.

In-situ heating experiments

The in-situ heating measurements were also performed on a FEI Talos F200X operated at 200 kV using a heating holder from DENSsolutions. The $Au@Ag@SiO_2$ NR solution was dropcasted on a heating chip consisting of several SiN windows. Once a suitable spot was chosen the chip was heated to 600 °C or 800 °C for the $Au@Ag@SiO_2$ and $Au@Pd@SiO_2$/$Au@Pt@SiO_2$ samples, respectively. The temperature was changed in steps of 50 °C and kept for about 5 min. The temperature increase per step was almost instantaneous (<1 s). However, since EDX maps were taken for 15 min the chip was kept at specific temperatures for a longer time. For example, EDX maps were taken of the spot from Figure 1 and a spot on a different window for the $Au@Ag@SiO_2$ sample at 400 °C (Figure 1). Thus, the sample was effectively heated for 40 min at that temperature. The influence of heating time is further analysed in Figure S7.

The $Au@Ag@SiO_2$ NRs were heated in a similar way. EDX measurements were performed at 600 °C, 700 °C and 800 °C and thus at these temperatures the particles were heated for 20 min instead of 5 min. Complete alloying was observed after keeping the temperature at 800 °C for 10 min more, thus 30 min in total. The EDX measurement at 800 °C shown in Figure 6 was taken after these 30 min. This was done because 800 °C was the maximal heating temperature and thus we increased the heating time at 800 °C and not the temperature until alloying was observed.

EDX measurements and analysis of maps

All EDX measurements were also performed at a FEI Talos F200X. Each map was taken for 15 min to get a good signal-to-noise ratio. The obtained intensity maps were quantified by using the Cliff-Lorimer method. Only Au and Ag or Pd were used for the quantification while the other elements were used for deconvolution only. For clarity only the Au and Ag or Pd maps are shown in the paper and not the Si or O maps although the mesoporous-silica shell is always present. All EDX maps in the main manuscript and Supplementary Information are presented in atomic percent except for Figure S8 and S13 which show the intensity maps.

Oven heating experiments

For the oven heating experiments in N_2 and air, the Au@Ag@SiO_2 NRs were dropcasted on microscope glass slides (76×26 mm, Thermo scientific, Menzel-Gläser). The oven heating in N_2 was done in a tube oven (Thermolyne 79300 tube furnace). The sample was placed in a quartz tube and flushed with N_2 for 1 h at room temperature. Thereafter the sample was heated to 300 °C with a rate of 15 °C/ min under a constant N_2-flow. After keeping the temperature at 300 °C for 10 min, the sample was heated to 400 °C with a rate of 10 °C/min and kept at 400 °C for 60 min. For the oven heating experiments in air we used a static air oven (Carbolite). After preheating the oven the glass slide was inserted and heated at 400 °C for 30 min. As a control experiment, we also heated the Au@Ag@SiO_2 in air with a similar temperature program as used for the N_2 experiments, but this did not lead to a different result. The dimensions of the Au@Ag@SiO_2 NRs before and after heating in N_2 and air are summarized in Table S2. It can be seen that the particles heated under N_2 barely changed their aspect ratio although they seem to slightly have decreased in volume. However, a smaller amount of particles was available for TEM analysis after heating compared to before heating. As the volume and ratio of Au and Ag did not change during the in-situ measurements, we believe that the apparent volume loss is due to limited statistics. A clear difference can be seen, however, for particles heated in air where a drastic change in volume and aspect ratio occurred (see also Figure S11). We observed that the porous silica shell structure was preserved during heat treatment. In Figure S2 a bright field TEM image of alloyed AuAg NRs is shown after heating them to 500 °C in N_2. The mesopores in the silica shell are still present and are expected to be stable up to ∼800 °C[5].

Table S2: Dimensions and aspect ratios (AR) of Au@Ag@SiO_2, Au@Pd@SiO_2 and Au@Pt@SiO_2 NRs before and after heating in-situ, in N_2 air at 400 °C of 1 h, as determined from TEM analysis.

Sample ID	Length (nm)	Diameter (nm)	AR
Au@Ag@SiO_2 NRs before in-situ heating	76	25	3.0
Au@Ag@SiO_2 NRs after in-situ heating	74	27	2.7
Au@Ag@SiO_2 NRs before N_2 heating	73	27	2.7
Au@Ag@SiO_2 NRs after N_2 heating	65	26	2.5
Au@Ag@SiO_2 NRs before air heating	73	27	2.7
Au@Ag@SiO_2 NRs after air heating	42	25	1.7
Au@Pd@SiO_2 NRs before in-situ heating	73	22	3.3
Au@Pd@SiO_2 NRs after in-situ heating	71	22	3.2
Au@Pt@SiO_2 NRs before in-situ heating	57	18	3.2
Au@Pt@SiO_2 NRs after in-situ heating	53	18	2.9

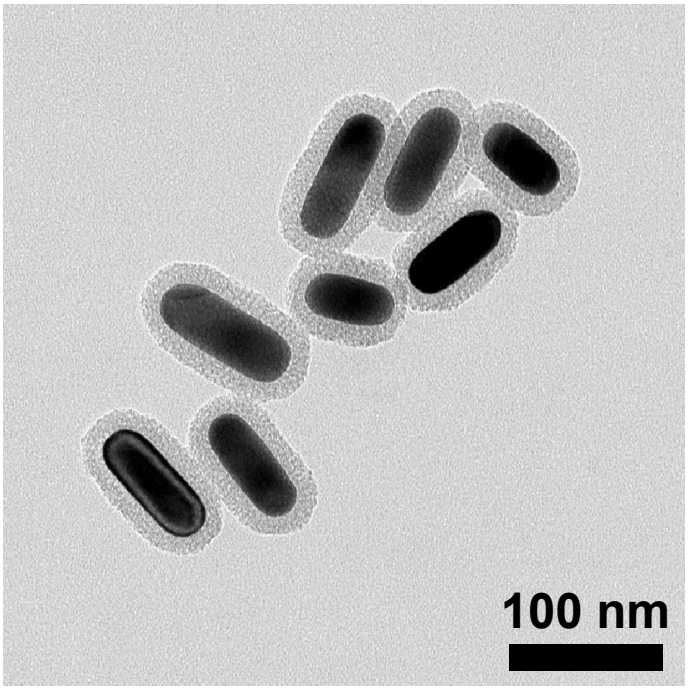

Figure S2: Bright field TEM image of mesoporous silica coated AuAg NRs after thermal treatment at 500 °C. The silica shell still has a mesoporous structure and was ∼15 nm thick before and after alloying.

Calculation of extinction spectra of alloyed NRs based on Mie-Gans theory

The extinction coefficients were calculated following Mie-Gans theory where the scattering (C_{sca}), absorption (C_{abs}) and extinction cross sections (C_{ext}) can be calculated from the polarizability α:

$$C_{sca} = \frac{k^4}{6\pi} |\alpha|^2 \tag{1}$$

$$C_{abs} = kIm(\alpha) \tag{2}$$

$$C_{ext} = C_{sca} + C_{abs} \tag{3}$$

$$\alpha_{x,y,z} = \frac{V(\epsilon_{AuAg} - \epsilon_d)}{\epsilon_d + L_{x,y,z}(\epsilon_{AuAg} - \epsilon_d)} \tag{4}$$

where $k = 2\pi\sqrt{\epsilon_d}/\lambda$ is the wave number, V the volume of the AuAg alloyed NR, ϵ_{AuAg} the complex dielectric function of the AuAg alloy and ϵ_d the dielectric constant of the surrounding dielectric medium. This analytical solution is valid for a spheroidal shape where the corresponding shape factors $L_{x,y,z}$ can be calculated by:

$$L_x = \frac{1-e^2}{e^2}\left(\frac{1}{2e} ln\left(\frac{1+e}{1-e}\right) - 1\right) \tag{5}$$

$$L_y = L_z = \frac{1 - P_A}{2} \tag{6}$$

$$e = \sqrt{1 - \frac{1}{AR^2}} \tag{7}$$

where e is the eccentricity and only depends on the aspect ratio AR of the NR. The factor L_x describes the behaviour along the long axis of the rod and thus is solely responsible for the longitudinal LSPR. Thus, we only calculated the longitudinal extinction coefficient. Prescott and Mulvaney determined the best shape factors for experimental rods and calculated the according values for different volumes, aspect ratios and end-cap geometries as those influence the spectra as well and not only the aspect ratio [6]. Following their approach we took a shape factor of $L_x = 0.092$ or $L_x = 0.118$ for the AuAg alloy NR which had an aspect ratio of 2.5 assuming a cylindrical or spherocylindrical shape, respectively. The dielectric constant of the surrounding medium ϵ_d was set to be 1.65. This value was determined by reproducing the measured extinction spectrum of the Au@SiO2 NRs dropcasted on a microscope slide before etching. Assuming a porosity of around 63% [7] an effective dielectric constant of SiO_2 and air (experimental conditions) would be 1.4. However, it needs to be considered that the pores are not just filled with air but that CTAB and condensed water in the pores increases the effective dielectric constant. Thus 1.65 is a reasonable value as it is inbetween 1.4 (silica and air) and 1.9 (silica and water). The value of ϵ_d was kept constant for all calculations as all measurements were performed on particles dropcasted on microscope slides.

The dielectric function of the AuAg alloy was taken from Rioux et al. [8] who developed an analytical model to obtain the dielectric function of AuAg alloys for all compositions. The dielectric functions were corrected for electron surface scattering which mainly influences the damping Γ_p [8,9]:

$$\Gamma_p(L_{eff}) = \Gamma_{pBulk} + A\frac{h\upsilon_F}{L_{eff}} \tag{8}$$

where Γ_{pBulk} is the damping parameter obtained for the bulk metal and $A\frac{h\upsilon_F}{L_{eff}}$ is a correction term to account for the modification of the mean free path due to the size confinement [8]. Hereby, υ_F is the Fermi speed of the free electrons ($1.4 \times 10^6\,\mathrm{ms}^{-1}$ for Au, Ag and their alloys) and L_{eff} the effective electron mean free path which can be calculated by $L_{eff} = 4 * V/S$ where S is the surface area of the particle and V its volume [9]. For the alloyed NRs from Figure 4 this results in L_{eff}=22.5 nm and in L_{eff}=25.6 nm for spheres of equal volume. In order to compare the influence of the shape we used the same V and L_{eff} for the cylindrical and spherocylindrical shape although V is a bit higher and L_{eff} slightly lower for the cylindrical shape (L_{eff}=21.7 nm). The surface scattering parameter A is often assumed to be 1 although different values were obtained in literature ranging from 0.3 to 1.4 [10–13]. To compare spherical and rod-shaped particles we chose A to be 1 for both cases. Figure S6 shows good agreement between the calculated extinction peak position for a composition of $x_{Ag} = 0.4$ (an experimental composition of $x_{Ag} = 0.44$ was determined by EDX) and the measured one. It is notable that the measured peak is broadened due to polydispersity and scattering of e.g. the silica shells.

The polarizability and thus the extinction coefficient for spherical particles can be calculated in a similar way following Mie theory:

$$\alpha_{x,y,z} = \frac{3V(\epsilon_{AuAg} - \epsilon_d)}{\epsilon_{AuAg} + 2\epsilon_d} \tag{9}$$

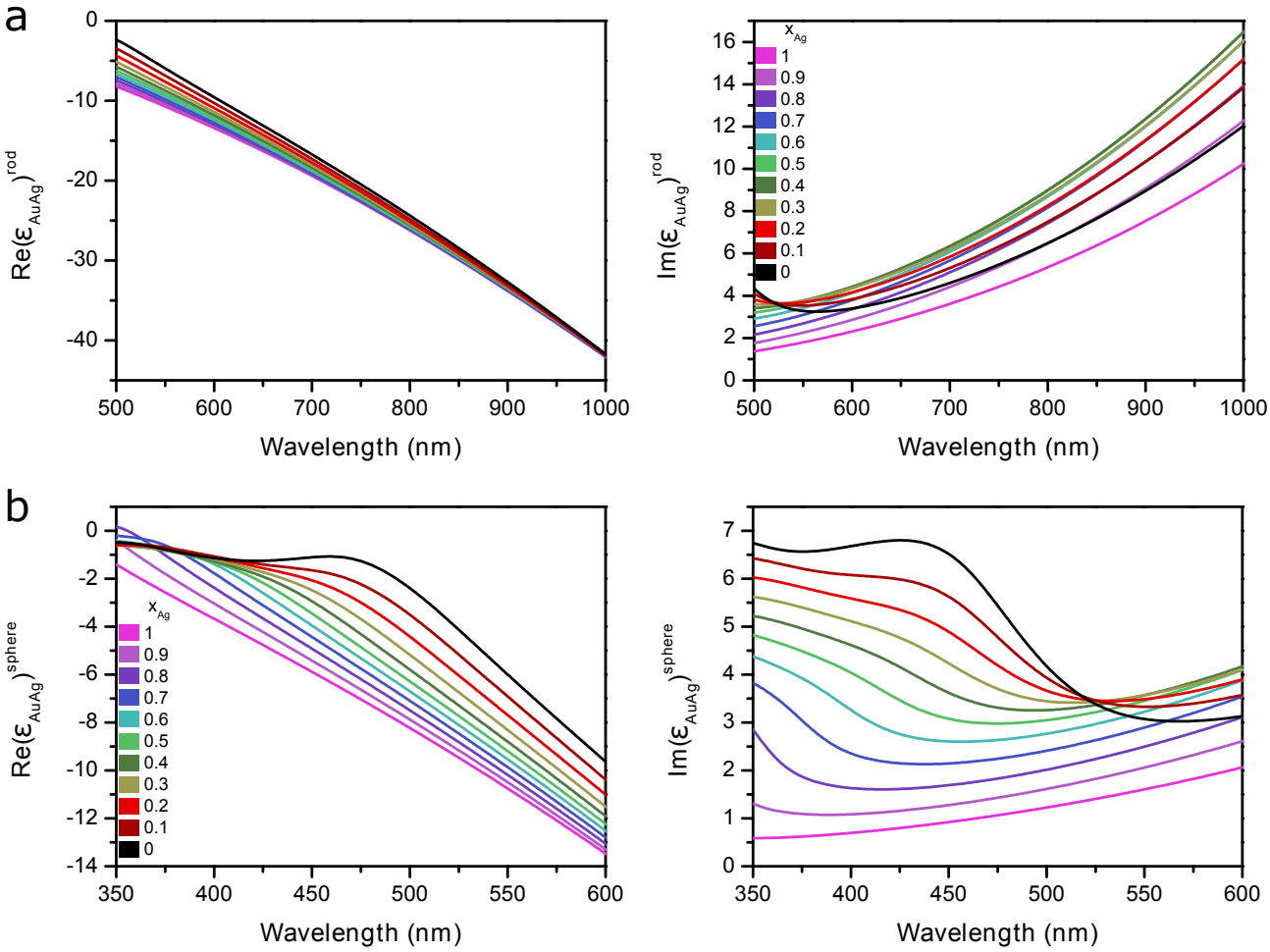

Figure S3: Calculated dielectric functions of AuAg alloys for different compositions. **a** Dielectric function for L_{eff}=22.5 nm (corresponding to the experimental AuAg alloy NRs obtained by heating Au@Ag@SiO_2 NRs in N_2, see Table S2 for dimensions). **b** Dielectric function for L_{eff}=25.6 nm (corresponding to spheres of the same volume as in a).

FDTD calculations

The FDTD calculations were performed with the software package Lumerical FDTD Solutions 8.15. A total field scattered field source was used and the longitudinal localized surface plasmon resonance was monitored at 200 points in a wavelength range from 500 nm to 1200 nm by aligning the polarization with the long axis of the NRs. A three-dimensional non-uniform mesh was used with a grid size of 0.5 nm for the NRs themselves and in their vicinity. The particles were either modelled as spherocylinders or cylinders using the experimentally determined sizes as presented in Table S2. The same dielectric functions and surrounding dielectric constant $\epsilon_d = 1.65$ as for the Mie-Gans calculations (Figure S3) were used.

Figure S4 compares the calculated extinction spectra for the core-shell Au-Ag NRs before heating to the alloyed NRs after heating under N_2. The NRs were modelled as spherocylinders and the dielectric function for a composition of $x_{Ag} = 0.4$ was used which was the experimentally determined composition of the NRs in Figure 4a. The longitudinal plasmon resonance blue-shifts after alloying due to the slight loss in aspect ratio. This confirms the experimental results in Figure 4a.

FDTD calculations were furthermore performed for all compositions x_{Ag} between 0 and 1 in 0.1 steps. Either a spherocylindrical or cylindrical shape with a length of 65 nm and a width of 26 nm was used. The results for a cylindrical shape are shown in the main paper in Figure 5 and the ones for the spherocylindrical shape are shown in Figure S5c and are very similar to the ones obtained with Mie-Gans theorydisplayed in the same Figure for a direct comparison. The peak position shifts and relative intensities are highly similar for all compositions

for the calculated extinction spectra obtained from FDTD (Figure S5c, Figure 5) and Mie-Gans calculations (Figure S5a and S5b). This shows that Mie-Gans theory can be used as a cheap and fast alternative to more difficult FDTD calculations. As a comparison the results for the spherical particle of the same volume as the nanorod are presented in the lower row where the intensities for the spherical alloy particles were normalized to the corresponding nanorod shape. Furthermore, it can be seen that the extinction for a completely spherical silver particle is overestimated for Mie-Gans theory compared to FDTD.

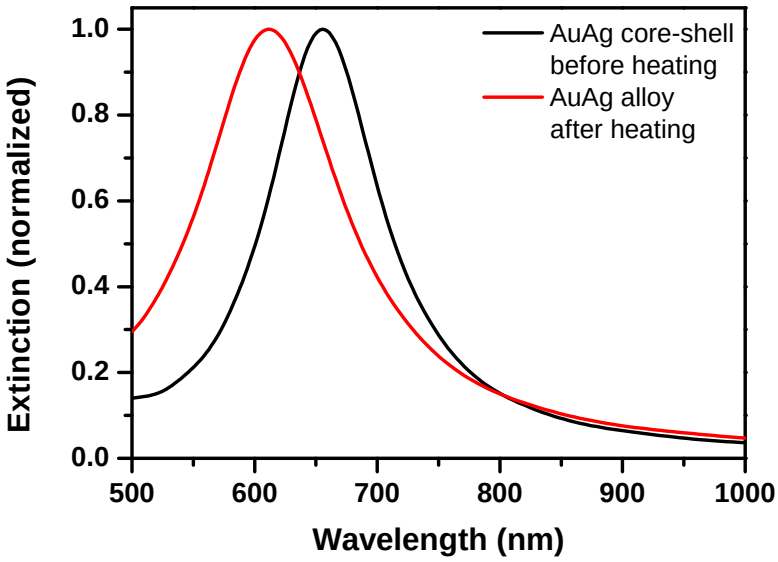

Figure S4: Comparison of the extinction spectra calculated for the core-shell Au-Ag NRs before heating (core length and width of 61 nm and 20 nm, respectively; shell length and width of 73 nm and 27 nm, respectively) and the alloy NR after heating (length and width of 65 nm and 26 nm, respectively) with a composition of $xAg = 0.4$. A spherocylindrical shape was assumed in both cases.

The results for a cylindrical and not spherocylindrical shape are presented in the main text because by comparing the experimental results to the calculated extinction spectra we found much better agreement for a cylindrical shape (Figure S6) despite the seemingly rather spherocylindrical shape observed from TEM for experimental rods. However, the small deformation of the NR shape after heating could probably also lead to a flattening of the tips resulting in a more cylindrical shape.

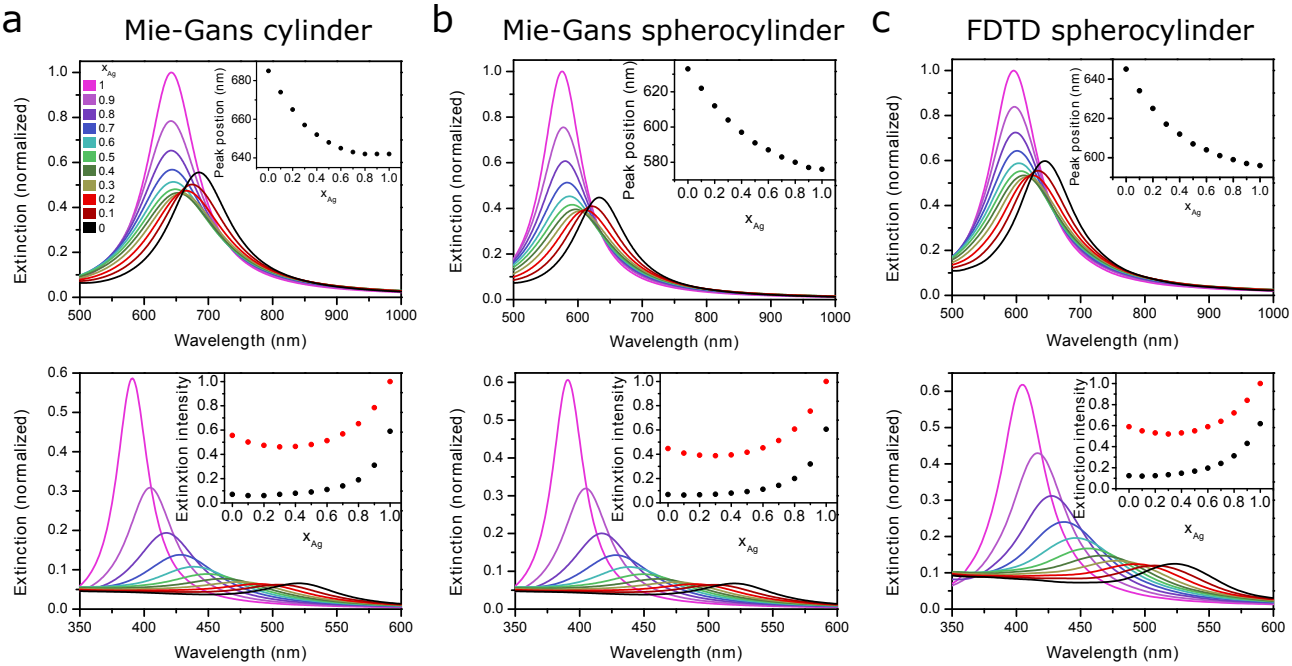

Figure S5: Comparison of extinction spectra for varying compositions x_{Ag} obtained from Mie-Gans and FDTD calculations. a) Mie-Gans calculations for a cylindrical shape ($L_x = 0.092$) b) Mie-Gans calculations for a spherocylindrical shape ($L_x = 0.118$) c) FDTD calculations for a spherocylindrical shape. The size of the nanorod was 65 nm × 26 nm for all cases. The lower row depicts the calculated spectra for a sphere of the same volume. For a and b these are the same graphs but the insets differ since the intensities of the nanorods are slightly different.

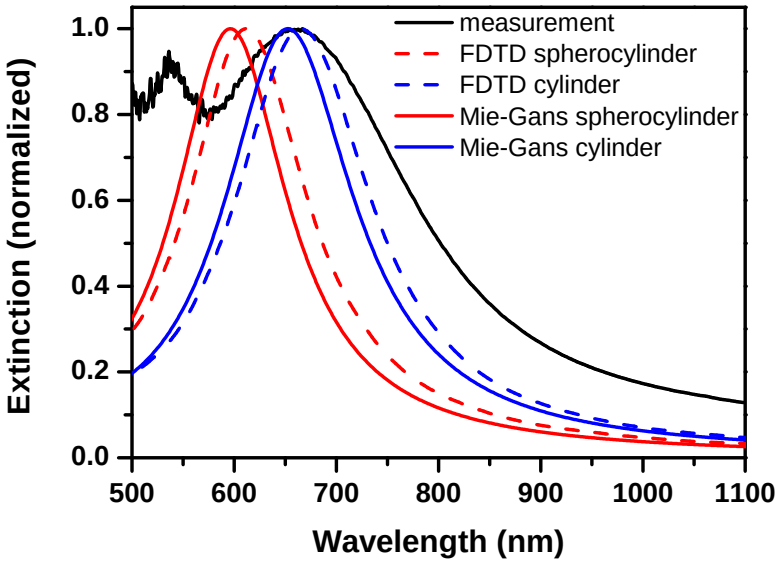

Figure S6: Comparison of the measured extinction spectrum for the alloy from Figure 4a (black curve) to the calculated extinction spectra for a cylindrical (blue) and spherocylindrical (red) shape and an alloy composition of $x_{Ag} = 0.4$. The size of the nanorod was in all cases 65 nm × 26 nm. Furthermore, the results for Mie-Gans (solid line) and FDTD (dashed line) calculations are compared.

In-situ heating

Next to the heating temperature, the heating time is an important parameter in the alloying process. Figure S7a shows the influence of heating time for a temperature of 400 °C. Right after changing the temperature to 400 °C a Au@Ag@SiO_2 NRs core-shell structure was still clearly visible (upper left image in Figure S7a). After 5 min the shell started to disappear but was still distinguishable from the core. After 5 min of heating the EDX

measurement presented in Figure 1 was started. As evident from those measurements the core was still mainly gold whereas the shell started to form an AuAg alloy. After the EDX measurements and thus after 20 min heating at 400 °C a core-shell structure was less visible (lower left image in Figure S7a). This was confirmed by EDX measurements of particles lying on a different SiN window shown in Figure S7b as most of the particles had formed an alloy. Finally, after 40 min no core-shell structure can be seen from the STEM contrast. Figure S7b also confirms that the electron beam had a neglectable influence on the alloying process as the particles in S7b were not exposed to the electron beam before and still showed the same behaviour as the illuminated spot in Figure 1. This is further confirmed by Figure S7c which shows STEM images of particles in different SiN windows after the in-situ heating process without prior electron beam exposure. The particles do not show a core-shell contrast anymore but one smooth contrast similar to the particles in Figure 1 after heating.

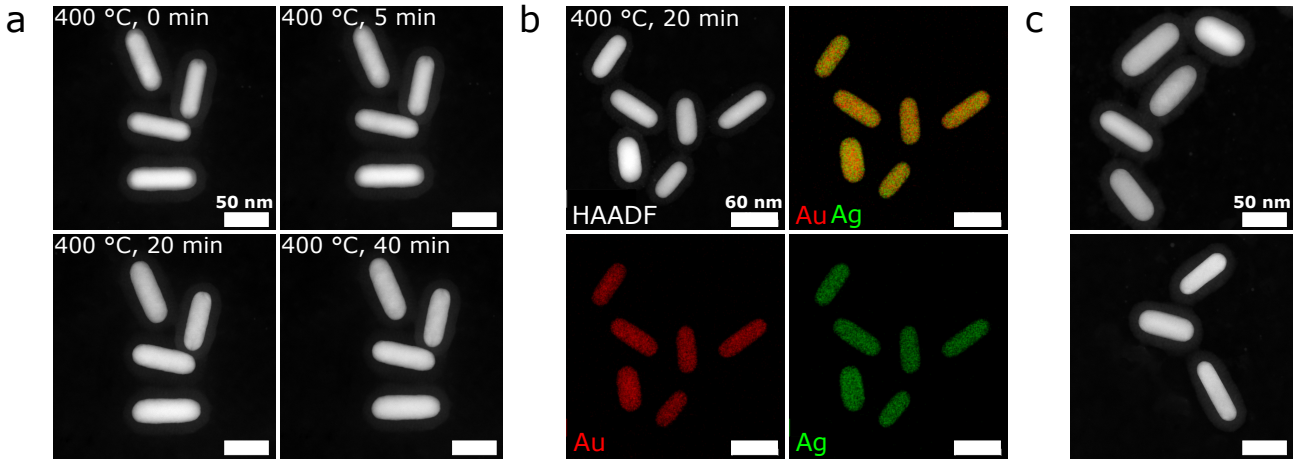

Figure S7: Influence of time and electron beam on the in-situ heating. a) Spot of Figure 1 after different times: directly after changing the temperature to 400 °C (0 min), after 5 min, after 20 min and after 40 min. b) EDX of a different spot on a different SiN window heated at 400 °C for 20 min without prior exposure to the electron beam. c) HAADF-STEM images of different spots on different SiN windows and thus without prior electron beam exposure after the end of the heating process.

Mesoporous silica

Figure S8 shows the intensity map of AuAg@SiO_2 NRs heated under nitrogen at 400 °C for 60 min (Figure 4a), including Si in the EDX map. It can be seen that also after heating the silica shell enclosed the AuAg rod.

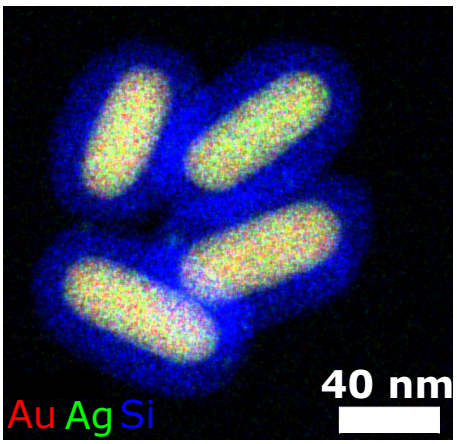

Figure S8: EDX intensity map of AuAg@SiO_2 NRs heated in N_2 for 60 min

EDX of etched Au@Ag@SiO_2 NRs

Figure S9 displays EDX measurements which confirm that the Au@Ag@SiO_2 NRs (before etching: L=73 nm, D=27 nm, AR=2.7) did not contain a Ag shell anymore after exposing them to an aquous mixture of 0.9 vol% NH_3 and 1.7 vol% H_2O_2 for 15 min. Here a not so representative spot was chosen where one particle still contained a small amount of Ag shell to make the difference clear.

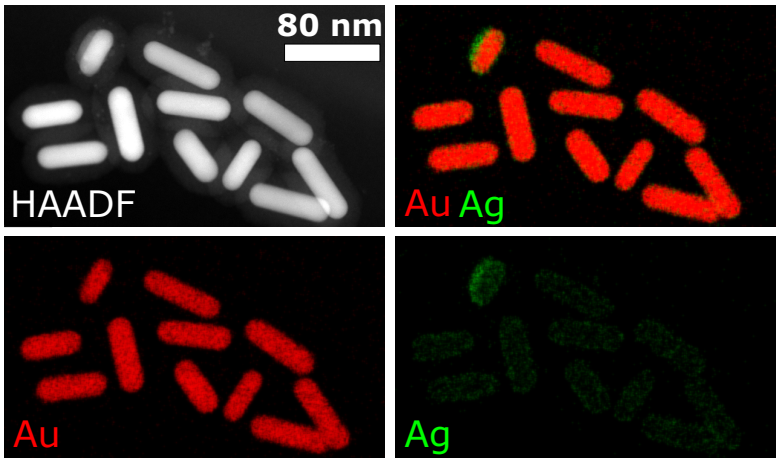

Figure S9: EDX map of etched Au@Ag@SiO_2 NRs.

Calculated extinction spectra for different aspect ratios

Figure S10 shows the calculated extinction spectra for 50/50 AuAg alloy NRs for aspect ratios ranging from 2 to 6. The volume is kept the same for all of the rods resulting L_x=0.113, 0.072, 0.053, 0.040 and 0.033 for AR=2, 3, 4, 5 and 6, respectively. The spectra are normalized to the one for an aspect ratio of 2. It can be seen that NRs with increasing aspect ratio exhibit higher extinction coefficients (up to 14 times higher compared to the spherical particles of the same volume in Figure 5) and red-shifted longitudinal LSPRs. Thus, the plasmonic properties of alloyed NRs can be further enhanced and tuned, with respect to spheres, by increasing the aspect ratio of the NR. Hence, by combining the possibility of tuning the aspect ratio and composition of the alloy NR, the whole VIS to NIR spectrum can be spanned.

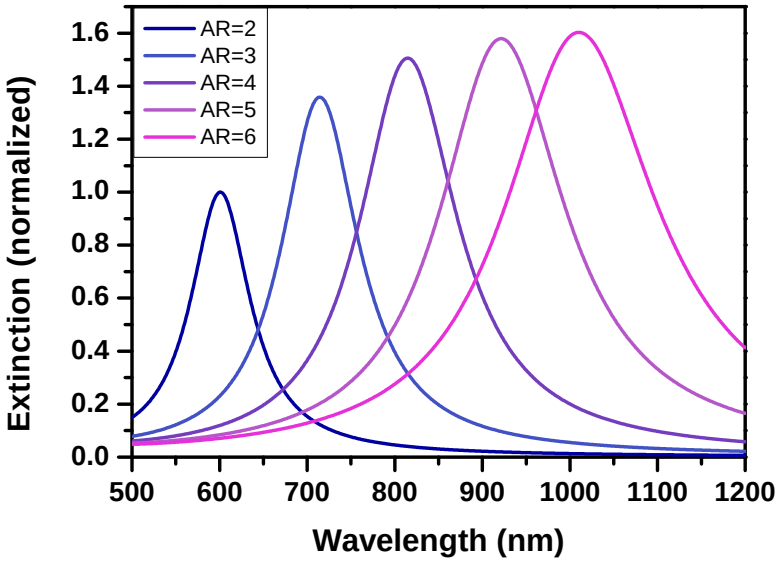

Figure S10: Calculated extinction spectra for AuAg alloyed NRs with $x_{Ag} = 0.5$ and varying aspect ratios (AR) of 2 to 6.

Deformation due to Ag loss

We found that most Ag vanished upon heating of Au@Ag@SiO_2 NRs in air leaving a void in the silica shell and thus space for the remaining Au NR to deform. Figure S11 shows Au@Ag@SiO_2 NRs after being heated in air for 30 min at 400 °C. The right NR still contained Ag, possibly due to blocked pores in the mesoporous SiO_2 shell which did not allow for mass transport, whereas the left particle contained mainly Au. The left particle deformed whereas the right one did not. This strengthens our hypothesis that particles deformed due to space being created in the silica shell after (partial) vanishing of the Ag.

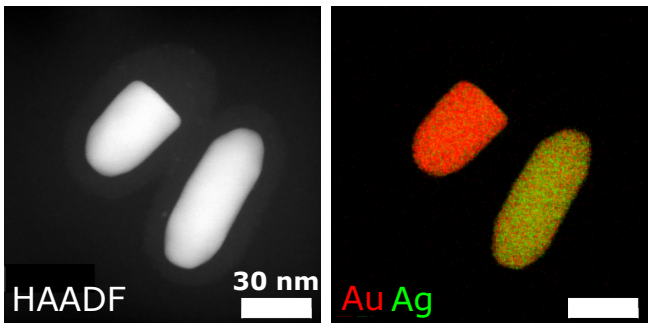

Figure S11: EDX map of two silica coated AuAg NRs after heating in air for 30 min at 400 °C.

Heating of monometallic Au@SiO_2 NRs

To compare the thermal stability of the bimetallic NRs to monometallic Au NRs we heated the Au@SiO_2 NRs (L=71 nm, D=20 nm, AR= 3.6) at 400 °C under a continuous N_2-flow for 60 min. In Figure S12 the extinction spectra before and after heat treatment are shown, both measured in air. The LSPR peak shifted from 748 nm to 716 nm indicating that the rods deformed to lower aspect ratios during heat treatment. The particle dimensions, as determined from TEM analysis, confirm the deformation (after heating: L=64 nm, D=20 nm and AR=2.9). The degree of deformation was higher compared to the Au@Ag@SiO_2 nanorods, which decreased in aspect ratio from 2.8 to 2.4 despite the similar volume. This could indicate that the thermal stability of AuAg alloyed NRs is slightly enhanced with respect to Au NRs, but could also ascribed to the difference in aspect ratio between the two samples.

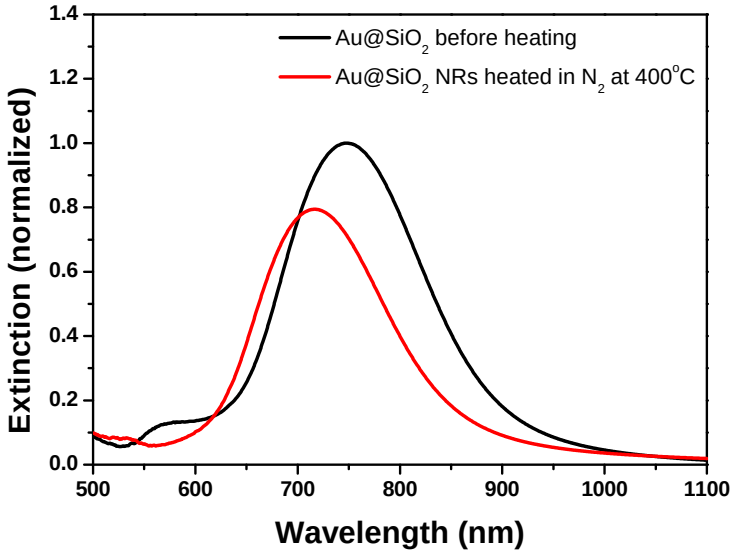

Figure S12: Extinction spectra of Au@SiO_2 NRs before (black, L=71 nm, D=20 nm, AR= 3.6) and after heating 60 min at 400 °C in N_2 (red, L=64 nm, D=20 nm and AR=2.9).

In-situ heating Au@Pt@SiO_2 nanorods

The alloying method presented in this paper can be applied to a variety of metals. Apart from Au@Ag@SiO_2 and Au@Pd@SiO_2nanorods, we also successfully alloyed core-shell Au@Pt@SiO_2 nanorods. Au@Pt@SiO_2 rods with Au/Pt=0.85/0.15 and L=57.2, D=17.6 nm, AR=3.2 were heated in-situ in the electron microscope. The HAADF-STEM image and EDX intensity maps in Figure S13 show the AuPt nanorods before, during and after heating to 800 °C. At 700 °C the core-shell structure vanished and an alloy was formed. The AuPt nanorods showed an extraordinary high thermal stability and only deformed slightly when heating to 800 °C (Au/Pt=0.85/0.15 and L=53.3, D=18.1 nm, AR=2.9).

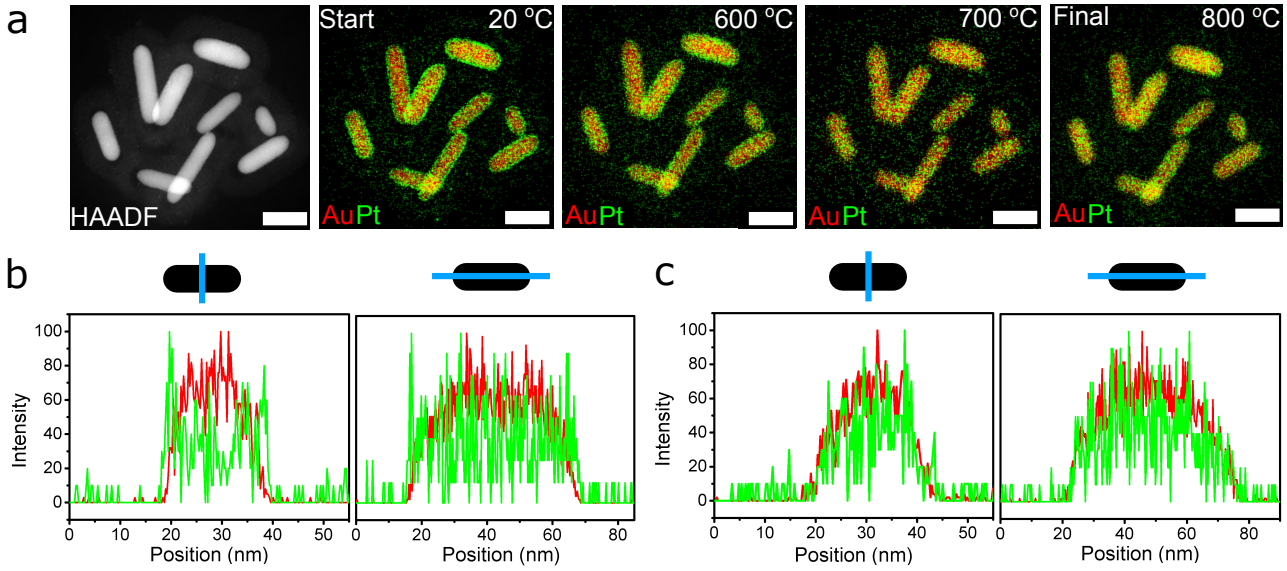

Figure S13: In-situ heating of Au@Pt@SiO_2 core-shell rods (Au/Pt=0.85/0.15 and L=57.2, D=17.6 nm, AR=3.2). a) HAADF-STEM image and EDX intensity maps showing the Au (red) and Pt (green) metal distribution before, during and after heating to 800 °C. The average aspect ratio of the 9 particles shown here changed from 3.2 to 2.9 when heating to 800 °C. The scale bars are 40 nm. b) EDX line scan of the upper right AuPt nanorod at 20 °C and c) after heating to 800 °C and cooling to room temperature.

References

[1] X. Ye, C. Zheng, J. Chen, Y. Gao and C. B. Murray, *Nano Lett.*, 2013, **13**, 765–771.

[2] I. Gorelikov and N. Matsuura, *Nano Lett.*, 2008, **8**, 369–73.

[3] T.-S. Deng, J. E. S. van der Hoeven, A. O. Yalcin, H. W. Zandbergen, M. A. van Huis and A. van Blaaderen, *Chem. Mater.*, 2015, **27**, 7196–7203.

[4] T.-S. Deng, J. E. S. van der Hoeven, W. Albrecht, A. O. Yalcin, F. D. Tichelaar, P. E. de Jongh, M. A. van Huis and A. van Blaaderen, *submitted*, 2017.

[5] C.-Y. Chen, S. L. Burkett, H.-X. Li and M. E. Davis, *Microporous Materials*, 1993, **2**, 27–34.

[6] S. W. Prescott and P. Mulvaney, *J. Appl. Phys.*, 2006, **99**, 123504.

[7] M. Grün, K. Unger, A. Matsumoto and K. Tsutsumi, *Microporous and Mesoporous Materials*, 1999, **27**, 207–216.

[8] D. Rioux, S. Vallières, S. Besner, P. Muñoz, E. Mazur and M. Meunier, *Adv. Opt. Mater.*, 2014, **2**, 176–182.

[9] E. A. Coronado and G. C. Schatz, *J. Chem. Phys.*, 2003, **119**, 3926–3934.

[10] C. Novo, D. Gomez, J. Perez-Juste, Z. Zhang, H. Petrova, M. Reismann, P. Mulvaney and G. V. Hartland, *Phys. Chem. Chem. Phys.*, 2006, **8**, 3540–3546.

[11] V. Juvé, M. F. Cardinal, A. Lombardi, A. Crut, P. Maioli, J. Pérez-Juste, L. M. Liz-Marzán, N. Del Fatti and F. Vallée, *Nano Lett.*, 2013, **13**, 2234–2240.

[12] Y. R. Davletshin, A. Lombardi, M. F. Cardinal, V. Juvé, A. Crut, P. Maioli, L. M. Liz-Marzán, F. Vallée, N. D. Fatti and J. C. Kumaradas, *ACS Nano*, 2012, **6**, 8183–8193.

[13] H. Baida, P. Billaud, S. Marhaba, D. Christofilos, E. Cottancin, A. Crut, J. Lermé, P. Maioli, M. Pellarin, M. Broyer, N. Del Fatti, F. Vallée, A. Sánchez-Iglesias, I. Pastoriza-Santos and L. M. Liz-Marzán, *Nano Lett.*, 2009, **9**, 3463–3469.